AGU PUBLICATIONS

Geophysical Research Letters

RESEARCH LETTER
10.1002/2014GL060946

Key Points:
- Separated treatment of coarse- and fine-mode particles in a RTM
- Improvement of the mineral dust longwave, direct radiative forcing estimation
- Increase of the longwave forcing when the coarse mode predominates up to 20%

Correspondence to:
M. Sicard,
msicard@tsc.upc.edu

Citation:
Sicard, M., S. Bertolín, C. Muñoz, A. Rodríguez, F. Rocadenbosch, and A. Comerón (2014), Separation of aerosol fine- and coarse-mode radiative properties: Effect on the mineral dust longwave, direct radiative forcing, *Geophys. Res. Lett.*, *41*, 6978–6985, doi:10.1002/2014GL060946.

Received 28 JUL 2014
Accepted 23 SEP 2014
Accepted article online 26 SEP 2014
Published online 13 OCT 2014

Separation of aerosol fine- and coarse-mode radiative properties: Effect on the mineral dust longwave, direct radiative forcing

Michaël Sicard[1], Santi Bertolín[2], Constantino Muñoz[2], Alejandro Rodríguez[2], Francesc Rocadenbosch[1], and Adolfo Comerón[2]

[1]RSLab/IEEC-CRAE, Universitat Politècnica de Catalunya, Barcelona, Spain, [2]RSLab, Universitat Politècnica de Catalunya, Barcelona, Spain

Abstract An improvement of the estimation of mineral dust longwave, direct radiative forcing is presented. It is based on recent developments that combine Sun photometer and multiwavelength lidar data to retrieve range-resolved coarse- and fine-mode extinction coefficients. The forcings are calculated separately for each mode, and their sum is compared to the classical approach in which only the total extinction is considered. The results of four cases of mineral dust intrusion in Barcelona, Spain, show that when the coarse mode predominates, the longwave forcings calculated with the classical approach are underestimated up to 20% near the surface. In all cases the strong coarse-mode predominance near the surface has also an effect on the forcing in the upper layers.

1. Introduction

Atmospheric aerosols directly and through their interactions with clouds contribute to the largest uncertainties in the estimation of the Earth's changing energy budget [*Intergovernmental Panel on Climate Change*, 2013]. Many radiative transfer models (RTMs) have been developed to locally estimate the aerosol direct radiative forcing (RF) [*Ricchiazzi et al.*, 1998; *Key and Schweiger*, 1998; *Mayer and Kylling*, 2005; *Berk et al.*, 2006]. In the longwave (LW) spectral range, the aerosol radiative properties are usually estimated theoretically with a Mie code. The variable that contains the absorption and scattering quantities, the extinction coefficient, is normalized to the extinction coefficient in the shortwave (SW) spectral range, most of the time in the visible spectral range [*Dufresne et al.*, 2002; *Sicard et al.*, 2014], or to the number concentration [*Sokolik et al.*, 1998]. As measurements of the extinction coefficient or its integral, the aerosol optical depth (AOD), are available in the SW spectral range, the equivalent extinction coefficient or AOD in the LW spectral range can be deduced thanks to that theoretical normalized extinction coefficient.

Since relatively little, the EARLINET (European Aerosol Research Lidar Network)/ACTRIS (Aerosols, Clouds, and Trace Gases Research Infrastructure Network—www.actris.net) community has developed codes that combine Sun photometer and lidar data to retrieve a set of variables vertically resolved related to the size distribution (fine- and coarse-mode extinction coefficients, fine- and coarse-mode volumetric concentrations, etc.): LIRIC (Lidar-Radiometer Inversion Code) [*Chaikovsky et al.*, 2012] and Generalized Aerosol Retrieval from Radiometer and Lidar Combined Data [*Lopatin et al.*, 2013]. Those codes are simpler than the ill-posed retrievals developed since the end of the 1990s [*Müller et al.*, 1999; *Veselovskii et al.*, 2002; *Böckmann et al.*, 2005] and work during daytime only. The objective of this paper is to check how the knowledge of the vertically resolved fine- and coarse-mode AOD modifies the LW RF. We concentrate on observations made in Barcelona, Spain, and on the case of mineral dust (MD) whose size distribution is often dominated by the coarse mode, which is the main contributor to the total LW RF [*Kinne and Pueschel*, 2001; *Myhre et al.*, 2003], as opposed to the fine mode which is the main contributor to the total SW RF [*Zhou et al.*, 2005].

2. Description of the LW RF Calculation

The calculation of the aerosol longwave radiative forcing is usually a two-step process: first a Mie code is used to spectrally calculate the aerosol radiative properties in the LW domain and second a radiative transfer model is used for the calculation of the RF.

2.1. Calculation of MD Radiative Properties in the LW Domain

The calculation of the aerosol radiative properties requires knowing the aerosols' shape, refractive index, size distribution, and density. *Yang et al*. [2007] showed that the nonsphericity effect of dust particles is not significant at the thermal infrared wavelengths which allow us (1) to assume that the shape of the MD is spherical and therefore (2) to use a Mie code. The real and the imaginary part of the refractive index of MD particles as a function of wavelength in the LW has been taken from measurements performed in Meppen in western Germany [*Volz*, 1983] on samples explicitly representative of transported MD. The table giving the refractive index as a function of wavelength can be found in *Krekov* [1993]. A discussion on the spectral behavior of the real and the imaginary part of the refractive index compared to the literature is given in *Sicard et al*. [2014]. The spectral refractive index is assumed constant independently of the size distribution. The MD size distribution is modeled using a bimodal lognormal distribution parameterized by volumetric radii, r_V, and standard deviations, σ_V, as well as volumetric concentrations, C_V. Those parameters are retrieved from AERONET (Aerosol Robotic Network) [*Holben et al*., 1998] Sun photometer measurements in Barcelona and thus are column-integrated values. We have paid a special attention to select cases with high MD loads (see section 3) so that the columnar size distribution is believed to be representative of MD. Finally, the MD particle density has been taken as 2.6 g cm^{-3} [*Hess et al*., 1998]. The aerosol vertical distribution was retrieved by means of lidar-derived extinction profiles.

2.2. The Radiative Transfer Model

Irradiances in the longwave spectral region have been calculated using the GAME code [*Dubuisson et al*., 2004, 2006]. GAME allows one to calculate upward and downward fluxes, *F*, in 40 vertical levels between the ground and 100 km, and at a fixed spectral resolution ($\Delta\nu = 20$ cm^{-1}) over the whole infrared spectral range. Aerosol forcing has been calculated as follows:

$$\Delta F_{\mathrm{BOA}} = \left(F^{w}_{\mathrm{BOA}}\downarrow - F^{w}_{\mathrm{BOA}}\uparrow\right) - \left(F^{o}_{\mathrm{BOA}}\downarrow - F^{o}_{\mathrm{BOA}}\uparrow\right) \quad (1)$$

and

$$\Delta F_{\mathrm{TOA}} = \left(F^{w}_{\mathrm{TOA}}\downarrow - F^{w}_{\mathrm{TOA}}\uparrow\right) - \left(F^{o}_{\mathrm{TOA}}\downarrow - F^{o}_{\mathrm{TOA}}\uparrow\right), \quad (2)$$

where F^w and F^o are the radiative fluxes with and without aerosols, respectively. The ↓ and ↑ arrows indicate if the fluxes are downward or upward, respectively. With this convention, a negative sign of the daily ΔF implies an aerosol cooling effect. GAME accounts for thermal emission, absorption, and scattering, as well as their interactions, using the Discrete Ordinates Method (discrete ordinates radiative transfer) [*Stamnes et al*., 1988]. Gaseous absorption (H_2O, CO_2, O_3, N_2O, CO, CH_4, and N_2) is treated from the correlated *k* distribution [*Lacis and Oinas*, 1991]. The spectral optical properties of aerosols are defined for each atmospheric layer, including the extinction optical depth, the single scattering albedo, and the asymmetry factor.

The atmospheric variables such as pressure, temperature, and relative humidity were measured by radiosoundings at 1200 UT of the corresponding day. The surface albedo, ε, was calculated from the surface emissivity, ρ, available in the Single Scanner Footprint (SSF) Level2 products of the CERES (Clouds and the Earth's Radiant Energy System) sensor in the spectral range of its WN "window" from 8.1 to 11.8 μm as $\varepsilon = 1 - \rho$. The surface temperature was taken directly from the SSF Level2 products of CERES. Because CERES SSF Level2 products are given for a spatial resolution equivalent to its instantaneous footprint, 38 by 31 km at nadir, which covers a large area encompassing the city of Barcelona, they are representative of a mixture of ocean and land [*Sicard et al*., 2014].

2.3. LW RF Calculation

2.3.1. The Classical Approach

Up to now, the most accurate way to get the vertical distribution of aerosol LW radiative properties on a routine basis (airborne measurements are omitted) is to calculate those properties with a Mie code from a measured size distribution (e.g., from a Sun photometer) and get the vertical distribution thanks to a lidar-derived extinction profile. In Barcelona, the AERONET column-integrated size distribution in cases of MD intrusions is always bimodal with a fine and a coarse mode [*Basart et al*., 2009]. Assuming the other parameters (shape, refractive index, and density) from section 2.1 and the AERONET bimodal size distribution, a Mie code allows for the calculation of the MD spectral radiative properties in the longwave spectral range, in particular the normalized extinction coefficient (normalized to the extinction coefficient at 532 nm), the single scattering

albedo (SSA) and the asymmetry factor, g. The lidar-derived total extinction profile at 532 nm is used to distribute vertically the total AOD, $AOD_t^{lidar}(z)$. The extinction coefficient was retrieved by means of the two-component elastic lidar inversion algorithm [*Fernald*, 1984; *Sasano and Nakane*, 1984; *Klett*, 1985] constrained with the Sun photometer-derived AOD [*Reba et al*., 2010]. The method is based on an iterative lidar ratio search by comparing the lidar AOD with that from the Sun photometer using a bisection-search method and a lidar ratio termination error goal set by the user [*Reba et al*., 2010].

In GAME the longwave, normalized extinction coefficient is multiplied to the lidar-derived AOD profile, $AOD_t^{lidar}(z)$, to obtain an equivalent, range-resolved profile of total AOD in the LW spectral range. Both the SSA and the asymmetry factor are assumed constant with height. Finally, GAME estimates the MD direct, total LW RF, noted ΔF^{class}.

2.3.2. Refinement by Separating the Fine and Coarse Modes

The LIRIC algorithm has been developed within EARLINET/ACTRIS by the Institute of Physics in Minsk (Belarus) in collaboration with the Laboratoire d'Optique Atmosphérique, Lille (France) [*Chaikovsky et al*., 2012]. LIRIC calculates the fine and coarse particle concentration profiles, using the backscattered lidar signals at three wavelengths (355, 532, and 1064 nm) and the column-averaged aerosol microphysical properties retrieved from the Sun photometer. The assumption is made that except for the concentration, all other particle properties are constant along the atmospheric column and equal to the column-averaged values provided by the Sun photometer. The retrieval is based on a maximum-likelihood estimation of the concentration profiles, so that the lidar signals are reproduced within their measurement uncertainty and the integral of the retrieved aerosol concentrations matches (within 5%) the total volume concentration of the fine and coarse modes derived from Sun photometric measurements. A detailed description of LIRIC can be found in *Chaikovsky et al*. [2012] and *Wagner et al*. [2013].

In the absence of cross-polarized channel (our case), the profiles of the extinction coefficients at 532 nm of the coarse and fine modes are given by the following:

$$\alpha_c(z) = C_{V,c}(z)a_c(532\ \text{nm}) \tag{3}$$

and

$$\alpha_f(z) = C_{V,f}(z)a_f(532\ \text{nm}), \tag{4}$$

where $C_V(z)$ denotes the range-resolved volume concentration and a the column mean value of the volume-specific particle extinction coefficient. The subscript c/f denotes either the coarse or the fine aerosol mode. Both variables $C_V(z)$ and a are direct outputs of the LIRIC code itself. By integrating those extinction profiles, one easily obtains the coarse- and the fine-mode AOD profiles, respectively, noted $AOD_c^{LIRIC}(z)$ and $AOD_f^{LIRIC}(z)$.

In this new approach, called the Mode Separation Profiling (MSP) method, the two modes are treated separately. Each mode (coarse and fine) is treated as a monomodal size distribution in the Mie code. For each set of normalized extinction and LIRIC-derived range-resolved AOD, we calculate the LW RF corresponding to the coarse mode, noted $\Delta F^{MSP,c}$, and to the fine mode, noted $\Delta F^{MSP,f}$. The sum of both forcings, noted $\Delta F^{MSP,t}$, gives the MD direct, total LW RF.

3. Real Cases and Discussion

The RF is estimated for four real cases of MD outbreaks in Barcelona which took place between 2010 and 2012. Only AERONET level 2 data are considered. MD particles have been discriminated by applying the method described in *Gobbi et al*. [2007] and *Basart et al*. [2009] that classifies the aerosols as MD when the Ångström exponent, $AE_{440,870}$, is less than 0.75, and the difference $\delta AE = AE_{440,675} - AE_{675,870}$ is less than 0.3. AE_{λ_1,λ_2} refers to the Ångström exponent calculated between the two wavelengths λ_1 and λ_2. To guarantee errors lesser than 30%, *Gobbi et al*. [2007] recommend to apply an additional criterion on the aerosol optical depth at 675 nm: $AOD > 0.15$.

The main characteristics of all four cases are listed in Table 1. The coarse mode appears clearly predominant in all cases. The fraction $C_{V,c}$ to $C_{V,f}$ varies between nearly 4 and 6. Case 4 is remarkable in the sense that the coarse mode shows a narrow peak ($\sigma_{V,c} = 0.545$) around $r_{V,c} = 1.809$ μm and that $C_{V,f}$ ($0.257\ \mu m^3 \cdot \mu m^{-2}$) is more than double the value of the other three cases. The AOD of Case 4, 0.48, is also more than double the AOD of the other three cases. The four cases are illustrated in Figure 1 in terms of time series of the

Table 1. Main Characteristics of the Four Cases for Which the MD Layer Radiative Properties Have Been Calculated[a]

					Coarse Mode			Fine Mode		
Case	Day	Time (UT)	AOD	CERES	$r_{V,c}$ (μm)	$\sigma_{V,c}$ ()	$C_{V,c}$ ($\mu m^3 \cdot \mu m^{-2}$)	$r_{V,f}$ (μm)	$\sigma_{V,f}$ ()	$C_{V,f}$ ($\mu m^3 \cdot \mu m^{-2}$)
1	12/04/2011	09:53	0.19 (08:40)	10:41	1.708	0.631	0.066	0.152	0.547	0.018
2	22/08/2011	18:05	0.23 (17:21)	10:17	1.953	0.588	0.101	0.131	0.503	0.026
3	01/09/2011	18:54	0.23 (17:06)	12:34	2.206	0.629	0.112	0.143	0.520	0.020
4	28/06/2012	18:47	0.48 (18:00)	12:04	1.809	0.545	0.257	0.117	0.647	0.042

[a]*Time* refers to the lidar start time (all lidar measurements are of a duration of 30 min). *AOD* is the AERONET AOD at 532 nm calculated from the AOD at 440 nm and the Ångström exponent calculated between 440 and 675 nm. The time in parenthesis is the AERONET measurement time. The column *CERES* indicates the overpass time of the CERES sensor. Dates in the column Day are formatted as day/month/year.

attenuated backscatter coefficient profiles as well as LIRIC-inverted extinction profiles (coarse mode, fine mode, and the sum of them). Error bars showing the uncertainty of the extinction coefficients due to the LIRIC algorithm have been computed. For this purpose, different user-defined input parameters (regularization parameters of the algorithm, complete overlap height, maximum height, and reference height) have been independently varied within reasonable limits to obtain different sets of retrievals [*Wagner et al.*, 2013; *Granados-Muñoz et al.*, 2014]. These variations have been kept within the limits for which the difference between the calculated column-integrated concentrations, and those provided by AERONET are not larger than 5%. The overall LIRIC uncertainty has been calculated considering the different user-defined input parameters as independent sources of error. Statistical uncertainties of the lidar data are around 15%

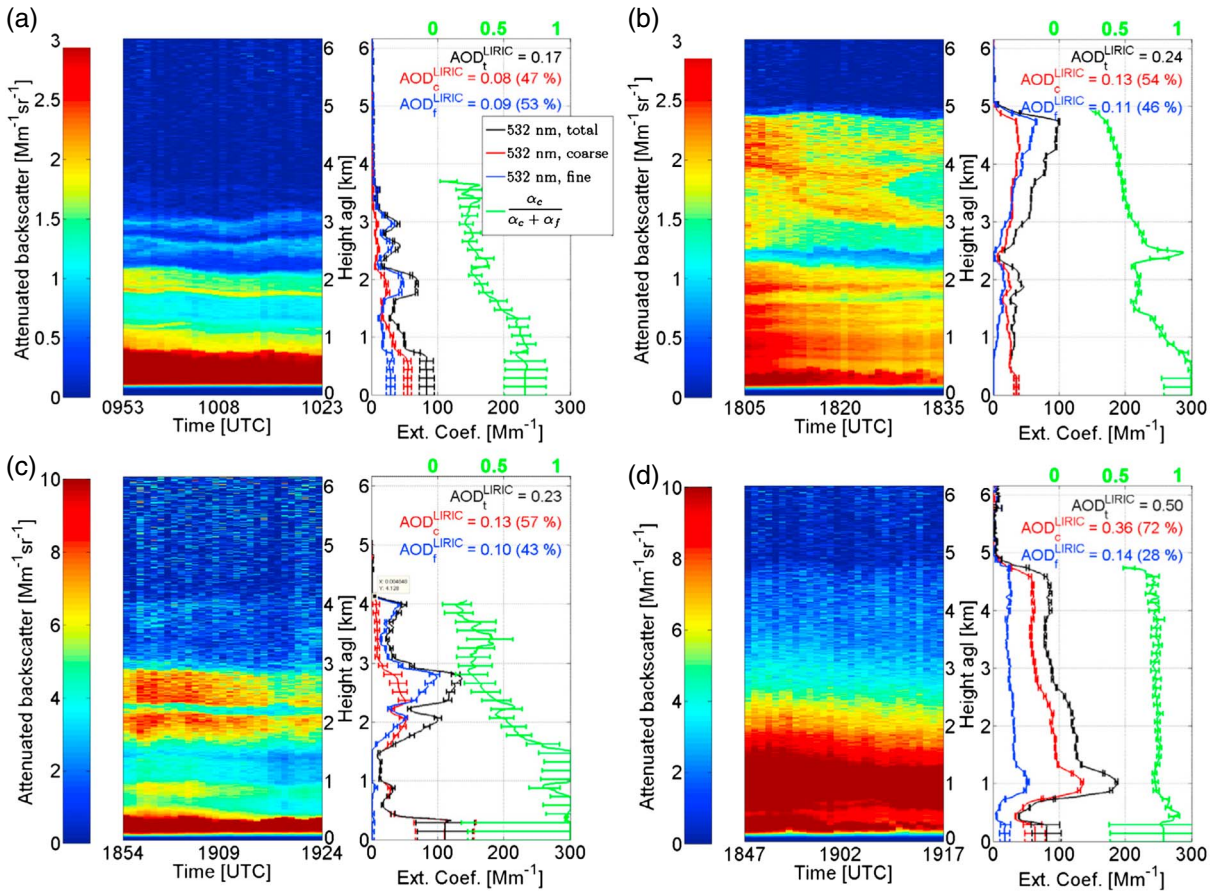

Figure 1. Time series of the attenuated backscatter coefficient profiles and LIRIC-inverted extinction profiles on (a) Case 1 (12 April 2011), (b) Case 2 (22 August 2011), (c) Case 3 (1 September 2011), and (d) Case 4 (28 June 2012). The legend in Figure 1a is the same for all the plots. The ratio $\frac{\alpha_c}{\alpha_c+\alpha_f}$ (0 if the fine mode predominates; 1 if the coarse mode predominates) is represented in green (upper axis). AOD_t^{LIRIC} represents the sum of AOD_c^{LIRIC} and AOD_f^{LIRIC}.

Table 2. LW RF Calculated With the Classical Approach (ΔF^{class}) and the New MSP Method ($\Delta F^{MSP,c}$, $\Delta F^{MSP,f}$, and Their Sum $\Delta F^{MSP,t}$)[a]

Case	Day	Time (UT)	AOD	ΔF^{class}_{BOA}	ΔF^{class}_{TOA}	$\Delta F^{MSP,c}_{BOA}$	$\Delta F^{MSP,c}_{TOA}$	$\Delta F^{MSP,f}_{BOA}$	$\Delta F^{MSP,f}_{TOA}$	$\Delta F^{MSP,t}_{BOA}$	$\Delta F^{MSP,t}_{TOA}$
				(W m^{-2})		(W m^{-2})		(W m^{-2})		(W m^{-2})	
1	12/04/2011	09:53	0.19	+2.8 (−10%)	+0.6 (+0%)	+2.7	+0.5	+0.4	+0.1	+3,1	+0,6
2	22/08/2011	18:05	0.23	+4.3 (−20%)	+2.2 (−4%)	+5.0	+2.0	+0.5	+0.3	+5.4	+2.3
3	01/09/2011	18:54	0.23	+3.7 (−16%)	+1.6 (+7%)	+4.0	+1.4	+0.4	+0.1	+4.4	+1.5
4	28/06/2012	18:47	0.48	+9.3 (−15%)	+4.2 (−16%)	+10.2	+4.7	+0.7	+0.2	+11.0	+5.0

[a]The percentages indicate the relative error produced by the estimation of the LW RF obtained with the classical method versus that obtained with the new method $\left(\frac{\Delta F^{class}-\Delta F^{MSP,t}}{\Delta F^{MSP,t}}\right)$. Dates in the column Day are formatted as day/month/year.

[*Pappalardo et al.*, 2004]. *Granados-Muñoz et al.* [2014] presents a summary of AERONET uncertainties of the optical and microphysical parameters used in the LIRIC inversion. Like *Granados-Muñoz et al.* [2014], we find that the largest LIRIC uncertainty is due to the complete overlap height and occurs in the lower part of the profiles. The overall LIRIC uncertainty reaches 40% in the first 500 m of the profile in Case 3. In that case, that can be considered as a limit case, an error on the extinction profile of 40% in the first 500 m produces an error on the AOD of ±0.022. According to *Sicard et al.* [2014], a variation of the AOD of ±0.022 roughly corresponds to a variation of the dust LW RF of ±0.33 and ±0.19 W m^{-2} at the bottom of atmosphere (BOA) and at the top of atmosphere (TOA), respectively.

In Figures 1a–1c a multilayer stratification is observed. The coarse-mode predominance in the bottom part of the MD layer decreases with increasing height. In the top part of the MD layer the fine mode predominates. In Figure 1d the MD layer is rather homogeneous: $\frac{\alpha_c}{\alpha_c+\alpha_f} \approx 0.72$ in the whole column and is nearly constant with height.

The calculations of the MD, direct LW RF are given in Table 2 for the classical approach and for the new MSP approach. The RF due to the fine mode is often less than 10% that of the coarse mode and never exceeds 15%, which is in agreement with *Sicard et al.* [2014]. To estimate the error committed on the estimation of the LW RF with the classical approach (when only the total AOD profile is available), we have calculated the relative error between ΔF^{class} and $\Delta F^{MSP,t}$. At the BOA where the coarse mode predominates (see Figure 1), the classical approach underestimates by 10 to 20% the total LW RF in all cases. At the TOA, the classical approach either overestimates (Case 3), compensates (Case 1), or underestimates (Cases 2 and 4) the total LW RF. This behavior seems linked to the degree of predominance of the coarse mode. As a comparison *Myhre et al.* [2003] found that underestimating the number of large MD particles could produce an underestimation of the regional (over western Africa) MD LW RF at the TOA up to 10 to 20%. In order to further investigate how the underestimation of ΔF^{class} links to coarse-mode predominance, we show in Figure 2 the MD radiative properties for the bimodal distribution (used in the classical approach), and for the coarse and fine modes (used in the MSP method). All four cases are represented on the plot of the normalized extinction. For the sake of clarity, only the properties of Case 1 are represented in the plot of the SSA and the asymmetry factor as the other cases give similar curves which almost overlap. One sees that the fine-mode LW normalized extinction does not vary significantly from one case to another. The coarse mode and the bimodal distribution vary up to a factor of 1.3 and 1.6, respectively, from one case to another. The coarse mode produces much larger LW normalized extinction values than the bimodal distribution. For Cases 1, 2, and 3 the coarse-mode LW normalized extinction is on average twice larger than that of the

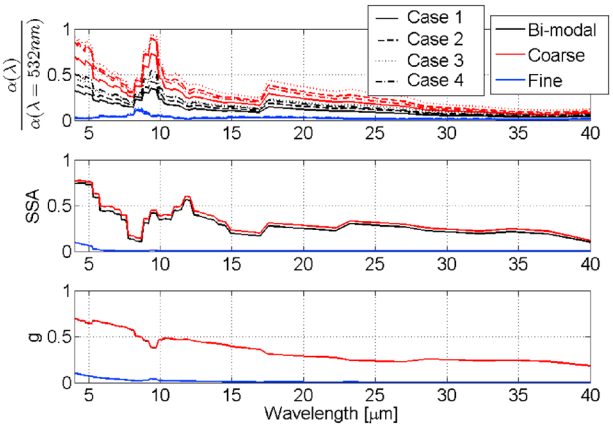

Figure 2. Mineral dust radiative properties as a function of wavelength for Case 1: (top) normalized extinction coefficient, (middle) single scattering albedo, and (bottom) asymmetry factor. The color legend in Figure 2 (top) is the same for all the plots. In the plot of the normalized extinction coefficient, the other cases are also represented.

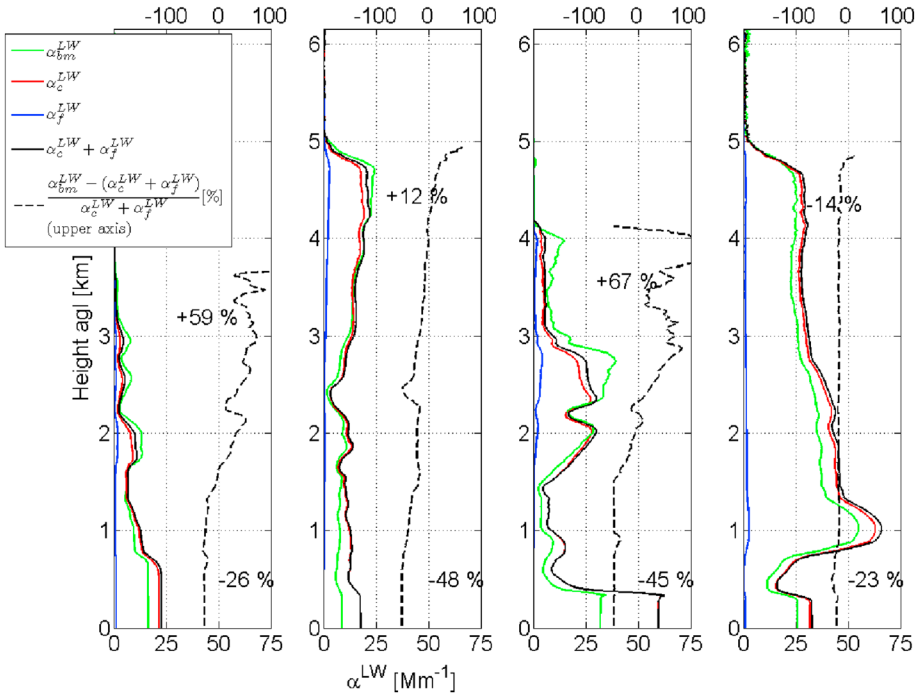

Figure 3. Longwave (in the range 8 to 13 μm) extinction coefficient for Cases1, 2, 3, and 4 (from left to right). The black dash line represents the percentage of $\frac{\alpha_{bm}^{LW}-(\alpha_c^{LW}+\alpha_f^{LW})}{\alpha_c^{LW}+\alpha_f^{LW}}$ (upper axis). The percentage numbers in each plot represent the mean value in the first and in the last kilometer of the profile.

bimodal distribution. For Case 4 that ratio decreases to 1.65 because of its relatively low ($r_{V,c}$ = 1.809 μm) and narrow ($\sigma_{V,c}$ = 0.545) coarse-mode radius. The association of those larger LW normalized extinction values with the profiles of the coarse-mode extinction coefficient at 532 nm (all predominated by the coarse mode: $\frac{AOD_c^{LIRIC}}{AOD_t^{LIRIC}} > 0.47$) might lead to profiles of LW extinction higher for the coarse mode than for the bimodal distribution. In order to check that hypothesis, we have averaged the normalized extinction coefficient (Figure 2) in the range 8–13 μm (the sensitive spectral window as far as radiative forcing is concerned) and multiply it by the corresponding extinction profile at 532 nm. The resulting profiles of the LW (in the range 8–13 μm) extinction coefficient, noted α^{LW}, are represented in Figure 3. The result of the classical approach is α_{bm}^{LW}, while $\alpha_c^{LW}+\alpha_f^{LW}$ is the result of the MSP method. In the bottom part of the MD layer where the coarse mode predominates (see Figure 1) α_{bm}^{LW} is always lower than $\alpha_c^{LW}+\alpha_f^{LW}$ (between −23 and −48%), resulting in a systematic underestimation of ΔF_{BOA}^{class} (see Table 2). In Cases 1, 2, and 3, in the top part of the MD layer, the fine mode predominates and α_{bm}^{LW} is larger than $\alpha_c^{LW}+\alpha_f^{LW}$ by +59, +12, and +67%, respectively. In Case 1, the strong LW extinction of the bimodal distribution (+59%) explains the compensation (+0%) of the LW RF at the TOA. In Case 3, α_{bm}^{LW} is even stronger (+67% with respect to $\alpha_c^{LW}+\alpha_f^{LW}$) and makes the classical approach to overestimate the LW RF at the TOA by 7%. In Case 2, the overestimation of α_{bm}^{LW} (+12%) is not sufficient to counteract the underestimation in the lowest part of the atmosphere since ΔF_{TOA}^{class} is still underestimated (−4%). This result indicates that the amount of large particles near the surface has also an effect on the forcing in the upper layers. In Case 4, in the top part of the MD layer, α_{bm}^{LW} keeps being lower than $\alpha_c^{LW}+\alpha_f^{LW}$ by −14%, which produces an underestimation of ΔF_{TOA}^{class} by 16%. One sees that the largest differences of α^{LW} at the surface (−45 and −48%) coincides with the highest underestimation of the LW RF (−16 and −20%, respectively) by the classical method. Those cases, Cases 2 and 3, give an idea of the maximum underestimation at the surface (−20%) caused by the use of the classical method since the coarse mode largely predominates at the surface ($\frac{\alpha_c}{\alpha_c+\alpha_f} \approx 1$; see Figure 1b).

4. Summary

Recent advances in combining synergistically Sun photometer and lidar data have direct applications in aerosol radiative forcing calculations and climate studies. By knowing the coarse-/fine-mode AOD vertical

distribution, the estimation of the aerosol LW RF gains in precision compared to the classical approach in which only the total AOD is known. In the mineral dust cases presented in this paper, the coarse-mode extinction coefficient in the LW spectral range is at least 1.65 higher than that of the corresponding bimodal size distribution. The largest differences are observed at the BOA where the coarse-mode predominance is stronger. There the classical approach underestimates up to 20% the LW RF estimated by separating the coarse and fine modes. In three of the four cases, the coarse-mode predominance at the surface evolves to a fine-mode predominance as height increases. In the two cases with the lowest ratio of coarse mode to total AOD, this evolution creates a compensation of the forcing at the TOA ($\Delta F_{\mathrm{TOA}}^{\mathrm{class}} = \Delta F_{\mathrm{TOA}}^{\mathrm{MSP},t}$) or even an overestimation ($\Delta F_{\mathrm{TOA}}^{\mathrm{class}} > \Delta F_{\mathrm{TOA}}^{\mathrm{MSP},t}$); in the third case, the LW RF remains underestimated by the classical method, indicating that the strong predominance of large particles near the surface has also an effect on the forcing in the upper layers. In one well-mixed case with a nearly constant ratio of coarse-mode to total AOD of 72%, the classical approach underestimates by ~15% the LW RF at the BOA and at the TOA.

Those results demonstrate that the radiative forcing produced by aerosols whose size distribution is dominated by the coarse mode is higher than that estimated by the classical method. This finding could lead to regional climate impacts less strong than what is estimated today (the longwave compensating the shortwave component) and to different behavior of the atmospheric circulation. This work underscores the importance of aerosol longwave forcing and motivates (i) the inclusion of the longwave component in the estimations of the aerosol direct radiative forcing in all kinds of RTM (local, regional, and global), especially in those cases where the aerosol coarse mode clearly dominates (e.g., near the sources); and (ii) the establishment of ground-based, aerosol multiwavelength lidar networks for the retrieval of the vertically resolved radiative properties of the aerosol coarse and fine modes.

Acknowledgments

This work is supported by the Seventh Framework Programme project Aerosols, Clouds, and Trace Gases Research Infrastructure Network (ACTRIS) (grant agreement 262254) and by the Spain-funded projects TEC2012-34575, UNPC10-4E-442, CGL2011-13580-E/CLI, and CGL2011-16124-E/CLI. The authors thank Philippe Dubuisson from Laboratoire d'Optique Atmosphérique (LOA), France, for the use of the radiative transfer model. The Earth Sciences Division of the Barcelona Supercomputing Center is acknowledged for the use of the Barcelona AERONET Sun photometer data.

Geoffrey Tyndall thanks Lucas Alados-Arboledas and two anonymous reviewers for their assistance in evaluating this paper.

References

Basart, S., C. Pérez, E. Cuevas, J. M. Baldasano, and G. P. Gobbi (2009), Aerosol characterization in Northern Africa, Northeastern Atlantic, Mediterranean Basin and Middle East from direct Sun AERONET observations, *Atmos. Chem. Phys.*, *9*, 8265–8282.

Berk, A., et al. (2006), MODTRAN5: 2006 update, *Proc. SPIE*, vol. 6233, 62331F, doi:10.1117/12.665077.

Böckmann, C., I. Miranova, D. Müller, L. Scheidenbach, and R. Nessler (2005), Microphysical aerosol parameters from multiwavelength lidar, *J. Opt. Soc. Am. A*, *22*, 518–528.

Chaikovsky, A., et al. (2012), Algorithm and software for the retrieval of vertical aerosol properties using combined lidar/radiometer data: Dissemination in EARLINET, in *Proceedings of the 26th International Laser and Radar Conference*, vol. 1, pp. 399–402, Porto Heli, Greece, 25–29 June.

Dubuisson, P., D. Dessailly, M. Vesperini, and R. Frouin (2004), Water vapor retrieval over ocean using near-infrared radiometry, *J. Geophys. Res.*, *109*, D19106, doi:10.1029/2004JD004516.

Dubuisson, P., J. Roger, M. Mallet, and O. Dubovik (2006), A code to compute the direct solar radiative forcing: Application to anthropogenic aerosols during the Escompte Experiment, in *Proceedings of the International Radiation Symposium (IRS 2004) on Current Problems in Atmospheric Radiation*, edited by H. Fischer and B. J. Sohn, pp. 127–130, A. Deepak Publ., Hampton, Va.

Dufresne, J., C. Gautier, and P. Ricchiazzi (2002), Longwave scattering effects of mineral aerosols, *Am. Meteorol. Soc.*, *59*, 1959–1966.

Fernald, F. G. (1984), Analysis of atmospheric lidar observations: Some comments, *Appl. Opt.*, *23*, 652–653.

Gobbi, G. P., Y. J. Kaufman, I. Koren, and T. F. Eck (2007), Classification of aerosol properties derived from AERONET direct Sun data, *Atmos. Chem. Phys.*, *7*, 453–458.

Granados-Muñoz, M. J., et al. (2014), Retrieving aerosol microphysical properties by Lidar-Radiometer Inversion Code (LIRIC) for different aerosol types, *J. Geophys. Res. Atmos.*, *119*, 4836–4858, doi:10.1002/2013JD021116.

Hess, M., P. Koepke, and I. Schult (1998), Optical properties of aerosols and clouds: The software package OPAC, *Bull. Am. Meteorol. Soc.*, *79*(5), 831–844.

Holben, B. N., et al. (1998), AERONET: A federated instrument network and data archive for aerosol characterization, *Remote Sens. Environ.*, *66*, 1–16.

Intergovernmental Panel on Climate Change (2013), *Climate Change 2013: The Physical Science Basis. Contribution of Working Group I to the Fifth Assessment Report of the Intergovernmental Panel on Climate Change*, edited by T. F. Stocker et al., Cambridge Univ. Press, Cambridge, U. K., and New York.

Key, J., and A. J. Schweiger (1998), Tools for atmospheric radiative transfer: Streamer and FluxNet, *Comput. Geosci.*, *24*(5), 443–451, doi:10.1016/S0098-3004(97)00130-1.

Kinne, S., and R. Pueschel (2001), Aerosol radiative forcing for Asian continental outflow, *Atmos. Environ.*, *35*, 5019–5028.

Klett, J. D. (1985), Lidar inversion with variable backscatter/extinction ratios, *Appl. Opt.*, *24*, 1638–1643.

Krekov, G. M. (1993), Models of atmospheric aerosols, in *Aerosol Effects on Climate*, edited by S. G. Jennings, pp. 9–72, Univ. of Ariz. Press, Tucson, Ariz.

Lacis, A., and V. Oinas (1991), A description of the correlated k-distribution method, *J. Geophys. Res.*, *96*, 9027–9064, doi:10.1029/90JD01945.

Lopatin, A., O. Dubovik, A. Chaikovsky, P. Goloub, T. Lapyonok, D. Tanré, and P. Litvinov (2013), Enhancement of aerosol characterization using synergy of lidar and Sun-photometer coincident observations: The GARRLiC algorithm, *Atmos. Meas. Tech. Discuss.*, *6*, 2253–2325, doi:10.5194/amtd-6-2253-2013.

Mayer, B., and A. Kylling (2005), Technical note: The libRadtran software package for radiative transfer calculations—Description and examples of use, *Atmos. Chem. Phys.*, *5*(7), 1855–1877, doi:10.5194/acp-5-1855-2005.

Müller, D., U. Wandinger, and A. Ansmann (1999), Microphysical particle parameters from extinction and backscatter lidar data by inversion with regularization: Theory, *Appl. Optics*, *38*, 2346–2357.

Myhre, G., A. Grini, J. M. Haywood, F. Stordal, B. Chatenet, D. Tanré, J. K. Sundet, and I. S. A. Isaksen (2003), Modeling the radiative impact of mineral dust during the Saharan Dust Experiment (SHADE) campaign, *J. Geophys. Res.*, *108*(D18), 8579, doi:10.1029/2002JD002566.

Pappalardo, G., et al. (2004), Aerosol lidar intercomparison in the framework of the EARLINET project. 3. Raman lidar algorithm for aerosol extinction, backscatter, and lidar ratio, *Appl. Opt.*, *43*, 5370–5385.

Reba, M. N. M., F. Rocadenbosch, M. Sicard, D. Kumar, and S. Tomás (2010), On the lidar ratio estimation from the synergy between AERONET Sun-photometer data and elastic lidar inversion, in *Proceedings of the 25th International Laser Radar Conference*, vol. 2, pp. 1102–1105, Saint Petersburg, Russia, 5–9 July.

Ricchiazzi, P., S. Yang, C. Gautier, and D. Sowle (1998), SBDART: A research and teaching software tool for plane-parallel radiative transfer in the Earth's atmosphere, *Bull. Am. Meteorol. Soc.*, *79*(10), 2101–2114, doi:10.1175/1520-0477(1998)079<2101:SARATS>2.0.CO;2.

Sasano, Y., and H. Nakane (1984), Significance of the extinction/backscatter ratio and the boundary value term in the solution for the two-component lidar equation, *Appl. Opt.*, *23*, 11–13.

Sicard, M., S. Bertolín, M. Mallet, P. Dubuisson, and A. Comerón (2014), Estimation of mineral dust longwave radiative forcing: Sensitivity study to particle properties and application to real cases in the region of Barcelona, *Atmos. Chem. Phys.*, *14*, 9213–9231, doi:10.5194/acp-14-9213-2014.

Sokolik, I. N., O. B. Toon, and R. W. Bergstrom (1998), Modeling the radiative characteristics of airborne mineral aerosols at infrared wavelengths, *J. Geophys. Res.*, *103*, 8813–8826, doi:10.1029/98JD00049.

Stamnes, K., S. Tsay, W. Wiscombe, and K. Jayaweera (1988), Numerically stable algorithm for discrete–ordinate-method radiative transfer in multiple scattering and emitting layered media, *Appl. Opt.*, *27*, 2502–2509.

Veselovskii, I., A. Kolgotin, V. Griaznov, D. Müller, U. Wandinger, and D. N. Whiteman (2002), Inversion with regularization for the retrieval of tropospheric aerosol parameters from multiwavelength lidar sounding, *Appl. Optics*, *41*, 3685–3699.

Volz, F. (1983), Infrared optical constants of aerosols at some locations, *Appl. Opt.*, *22*, 23.

Wagner, J., A. Ansmann, U. Wandinger, P. Seifert, A. Schwarz, M. Tesche, A. Chaikovsky, and O. Dubovik (2013), Evaluation of the Lidar/Radiometer Inversion Code (LIRIC) to determine microphysical properties of volcanic and desert dust, *Atmos. Meas. Tech.*, *6*, 1707–1724.

Yang, P., Q. Feng, G. Hong, G. W. Kattawar, W. J. Wiscombe, M. I. Mishchenko, O. Dubovik, I. Laszlo, and I. N. Sokolik (2007), Modeling of the scattering and radiative properties of nonspherical dust-like aerosols, *J. Aerosol Sci.*, *38*, 995–1014.

Zhou, M., H. Yu, R. E. Dickinson, O. Dubovik, and B. N. Holben (2005), A normalized description of the direct effect of key aerosol types on solar radiation as estimated from Aerosol Robotic Network aerosols and Moderate Resolution Imaging Spectroradiometer albedos, *J. Geophys. Res.*, *110*, D19202, doi:10.1029/2005JD005909.